Journal of Materials Chemistry A

PAPER

View Article Online
View Journal | View Issue

Cite this: J. Mater. Chem. A, 2018, 6, 6463

Stable hybrid organic–inorganic halide perovskites for photovoltaics from *ab initio* high-throughput calculations†

Sabine Körbel, ‡[a] Miguel A. L. Marques [b] and Silvana Botti *[ac]

Received 12th October 2017
Accepted 1st March 2018

DOI: 10.1039/c7ta08992a

rsc.li/materials-a

Hybrid perovskites, such as methylammonium lead iodide, have revolutionized research on solar cells in the past few years. Well known instability and toxicity issues restrain however the large-scale application of these perovskites in commercial photovoltaic technology. It is therefore the most urgent task to find a way to chemically stabilize these and other lead-free perovskites, preserving at the same time their excellent absorption and charge-transport properties. The obvious route to follow is chemical substitution. In this work we screen the periodic table of elements for hybrid organic–inorganic halide perovskites, using high-throughput density-functional theory calculations. We consider compounds with the composition $A^{+}B^{2+}X_3^{-}$, where A is a molecular organic cation, X is a halogen, and B is a divalent element. For the molecular cation, we vary the molecule size from sulfonium (H_3S, very small) to *tert*-butylammonium (C_4NH_{12}, very large). All thermodynamically stable hybrid perovskites are then further characterized by calculating their band gaps and effective masses, to identify the most promising candidates for further experimental and theoretical characterization. We find that the substitution of the organic molecule is the most promising way to enhance thermodynamic stability, while there is no optimal replacement for lead or Sn, unless one considers partial substitution or alloying.

1 Introduction

Perovskite absorbers have revolutionized research on solar energy with solar power conversion efficiencies that reached up to 22.1% (ref. 1) in only 6 years, through the optimization of perovskite-film fabrication and device architecture. In hybrid organic–inorganic perovskites, the large inorganic cations with 12-fold coordination are replaced by organic ions, preserving the characteristic octahedra of anions, which is typical for the perovskite crystal structure. Hybrid perovskites, whose best-known representative is methylammonium (MA) lead iodide $CH_3NH_3PbI_3$ ($MAPbI_3$),[2] are easy to manufacture, cheap, and highly efficient in converting light into electricity. However, known issues related to their inherent instability[3,4] (degradation when exposed to water, oxygen, UV-light, and high temperature) and toxicity (presence of lead) hinder the further development of perovskite-based solar cells over the long term.

This fact motivates the ongoing active search for new hybrid perovskites. An ideal candidate absorber should be thermodynamically stable, environmentally friendly, and preserve the excellent absorption and charge-transport properties of MA lead iodide. The obvious route to take is chemical substitution. However, repeated failed synthesis attempts in the lab made it clear that finding suitable substitutions relying only on simple empirical chemical rules and intuition is not an efficient strategy.

Several experimental studies have recently focused on obtaining stable hybrid perovskites. Indeed, a number of chemical substitutions have been attempted experimentally, such as replacing Pb by Sn.[4–6] Stoumpos *et al.* substituted Pb with Ge and also screened several organic molecules as potential substitutes for MA.[7] Mixed-molecule [MA + formamidinium (FA), MA + FA + Cs, and MA + ethylammonium (EA)] perovskites were successfully made.[8–10] Stability was found to improve when part of the I atoms are replaced by Br,[4,11] or by thiocyanate (SCN).[12] Moreover, partial substitution of BF_4 for I yielded better efficiency.[13] Even if these results are promising, a real breakthrough could not be achieved yet. Another strategy to stabilize the hybrid lead perovskite is to alloy it with an inorganic perovskite, such as $CsPbI_3$.[9,14–16]

The search for improved materials can also be tackled theoretically, using *ab initio* high-throughput calculations, as already put forward by various recent publications, focusing, *e.g.*, on inorganic perovskites,[17–19] materials for batteries,[20]

[a]Institut für Festkörpertheorie und -optik, Friedrich-Schiller-Universität Jena, Max-Wien-Platz 1, 07743 Jena, Germany. E-mail: skoerbel@uni-muenster.de; silvana.botti@uni-jena.de

[b]Institut für Physik, Martin-Luther-Universität Halle-Wittenberg, D-06099 Halle, Germany

[c]European Theoretical Spectroscopy Facility, Europe

† Electronic supplementary information (ESI) available: Tables with all calculation results. See DOI: 10.1039/c7ta08992a

‡ Current address: School of Physics and CRANN, Trinity College, Dublin 2, Ireland.

super-hard materials,[21] transparent conducting oxides,[22–24] organic polymer dielectrics,[25] and hard magnets,[26] to name just a few examples.

More specifically in the field of hybrid perovskites, a computational screening of possible replacements for methylammonium or lead was performed by Filip and coworkers,[27,28] while the substitution of the molecular anions BF_4 and PF_6 for I was studied in ref. 29. Jacobsson *et al.* investigated Sr replacement of Pb.[30] El-Mellouhi and coworkers showed that sulfonium (H_3S), methylsulfonium (CH_3–SH_2), and methylphosphonium (CH_3–PH_3) are very promising substitutions for MA, as they increase the thermodynamic stability while preserving the good electronic properties of $MAPbI_3$.[31,32] Methylphosphonium lead iodide had already been investigated by Filip and coworkers.[27] Jiang *et al.*[33] screened *in silico* many substitutions for Pb in $MAPbX_3$ (X = I, Cl, Br) and performed experiments to verify the calculated band gaps. Meng *et al.*[34] simulated the replacement of MA with several other molecular cations. Unfortunately, in all these studies only a small fraction of the possible search space was investigated, and/or the thermodynamic stability of the proposed compounds, or their possible decomposition into phases other than AX and BX_2, was neglected. Since thermodynamic stability is a crucial challenge in the field of hybrid perovskites, a broad study that focuses on both the thermodynamic stability and the electronic band structures of new hybrid organic–inorganic perovskites is called for. This is the objective of the present work.

To assess the thermodynamic stability of a compound, we calculate its distance from the convex hull of stability, *i.e.* we compare its formation enthalpy to that of all other known competing phases and phase mixtures, including decomposition into elemental, binary, ternary, and in our case also quaternary and quinternary phases. With the help of existing experimental and computational material databases and the public availability of efficient *ab initio* software based on density-functional theory (DFT), this task can be accomplished in an efficient way, allowing us to screen the whole periodic table to quickly identify stable candidates that deserve further attention.

Our goal is to propose substitutions for both Pb and the organic cation that (i) enhance thermodynamic stability, (ii) preserve small effective masses, and (iii) yield optimal band gaps for photovoltaics. In particular, we concentrate on halide perovskites of the form $A^+B^{2+}X_3^-$, where the molecular cation A

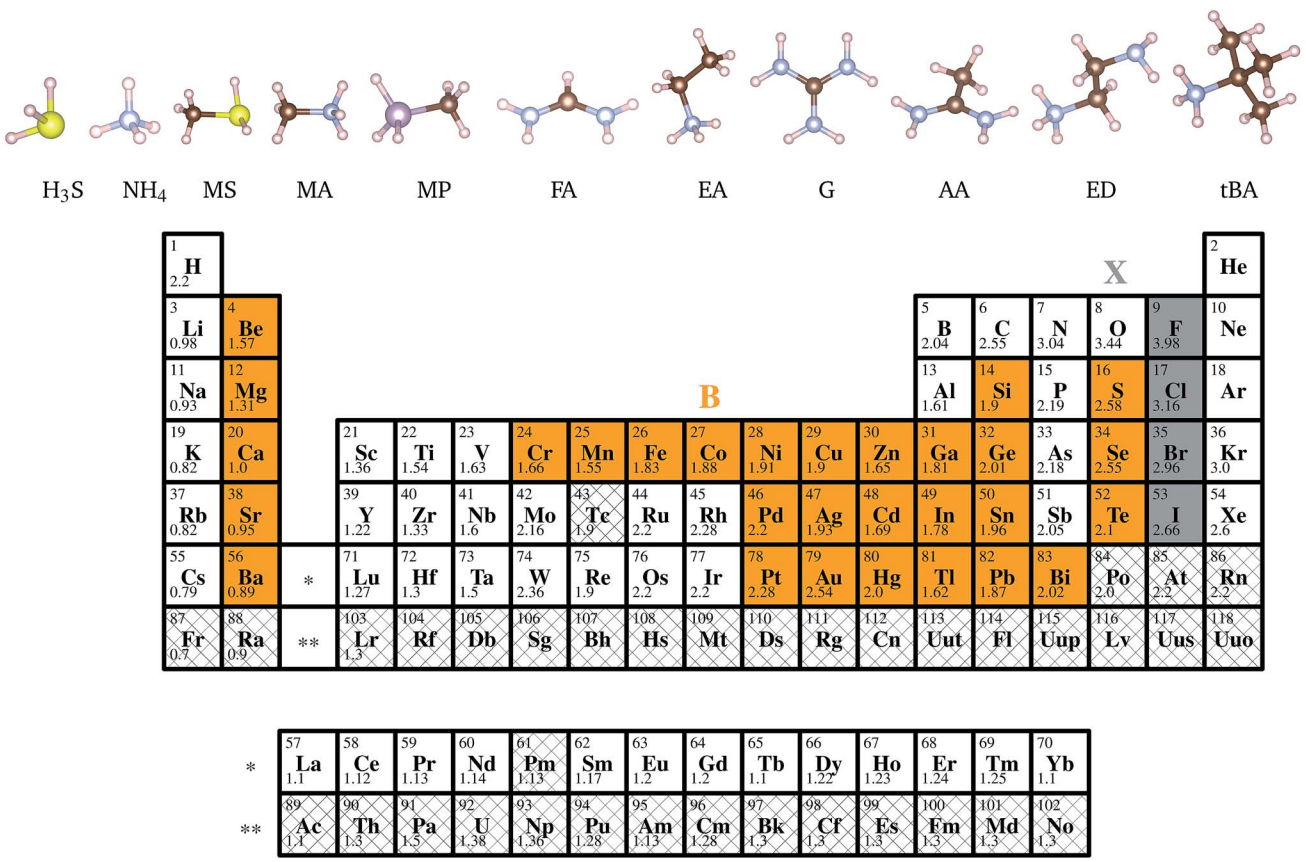

Fig. 1 Top: Molecular cations considered in this work ordered by size (from left to right): H_3S (sulfonium), NH_4 (ammonium), CSH_5 (methylsulfonium, MS), CNH_6 (methylammonium, MA), CPH_6 (methylphosphonium, MP), CN_2H_5 (formamidinium, FA), C_2NH_8 (ethylammonium, EA), CN_3H_6 (guanidinium, G), $C_2N_2H_7$ (acetamidinium, AA), $C_2N_2H_9$ (ethylenediamine, ED), and C_4NH_{12} (*tert*-butylammonium, *t*BA); hydrogen atoms are in pink, nitrogen ones blue, carbon ones brown, phosphorus ones gray, and sulfur ones yellow. Bottom: Periodic system of the elements with B (orange) and X elements (gray) considered for the ABX_3 compounds. The number in the lower left corner is the Pauling electronegativity. Radioactive elements are hatched.

is a small molecule, namely H_3S (sulfonium), NH_4 (ammonium), CSH_5 (methylsulfonium, MS), CNH_6 (methylammonium, MA), CPH_6 (methylphosphonium, MP), CN_2H_5 (formamidinium, FA), C_2NH_8 (ethylammonium, EA), CN_3H_6 (guanidinium, G), $C_2N_2H_7$ (acetamidinium, AA), $C_2N_2H_9$ (ethylenediamine, ED), or C_4NH_{12} (*tert*-butylammonium, *t*BA), X is F, Cl, Br, or I, and the divalent B element is Be, Mg, Ca, Sr, Ba, Cr, Mn, Fe, Co, Ni, Cu, Zn, Ge, Pd, Cd, In, Sn, Pt, Hg, Tl, Pb, S, Se, or Te (see Fig. 1). The molecular cations we chose have different sizes and elemental compositions and can therefore be regarded as a sampling of the vast space of small molecular cations. The idea of substituting Pb with trivalent ions (such as In) may appear surprising, but in fact substitution with diagonal neighbors in the periodic table is often successful.[35]

The remainder of this article is structured as follows: in Section 2, we describe our methodology and give the numerical parameters of the calculations. Section 3 contains the results for thermodynamic stability and electronic properties such as the band gaps and effective masses of the stable candidates. The paper closes with a summary and conclusion in Section 4. Tables with detailed numerical results are provided in the ESI.†

2 Methods

2.1 High-throughput setup

Our objective is to find solar-cell absorbers with absorption coefficients (in the frequency range of the solar spectrum that is most relevant for photovoltaics) and carrier mobilities as high as those of $MAPbI_3$. Moreover, we require that these compounds are lead-free and/or thermodynamically more stable than $MAPbI_3$. We now need to translate these requirements into descriptors suitable for an automatized computational screening. According to the Shockley–Queisser limit, the band gap size is directly related to the energy-conversion efficiency and is therefore a good descriptor. The electron and hole effective masses are simple descriptors related to the mobilities of charge carriers. Of course, high carrier mobilities are determined by both low effective masses and low scattering rates. The latter quantity is however too complex, as it depends on lattice vibrations, defects, and interfaces, and therefore cannot be calculated efficiently for a large set of materials. Finally, the energy of formation, if compared appropriately with all possible decomposition channels, determines the thermodynamic stability.

The three descriptors that we have identified are therefore (i) the size of the (direct) band gap, (ii) electron and hole effective masses, and (iii) the distance from the convex hull of stability. These descriptors are simple enough to allow for efficient large-scale calculations. The fact that the resulting candidate perovskites should ideally also be environmentally friendly (non-toxic elements and non-polluting elements) and cheap (not too rare or expensive elements) is then considered *a posteriori*.

Our procedure to identify promising stable hybrid ABX_3 compounds is as follows: we start with a fast, automatized screening of many compositions (11 molecules × 29 metals × 4 halogens = 1276 initial compounds) and successively apply filters while increasing the level of theory (all details are given in the next sections). First, we perform standard DFT calculations for all compounds using a perovskite crystal structure with only one formula unit per unit cell (we call it the "α" or "3D" phase). Second, we add a more complex perovskite crystal structure, the *Pnma* structure of orthorhombic $MAPbI_3$ (we call it the "3D–OR" phase), for only those compounds that are stable or moderately unstable (here we set the threshold for the distance from the convex hull of stability to 100 meV per atom; 646 intermediate compounds). Third, we add more prototype crystal structures for only those compounds that are stable within 10 meV per atom in one of the two perovskite crystal structures. Fourth, we characterize only those compounds which are (almost) stable (here the threshold is set to 10 meV per atom from the convex hull of stability; 203 stable compounds) more accurately. The band gap and effective masses are then evaluated for those compounds which passed through the last filter. The scheme is depicted in Fig. 3. All calculation steps (exchange of elements, structure optimization, filtering, graphical representation and tabulation of data) are automatized. Only the initial positioning of the organic molecule in the inorganic framework required some human guidance.

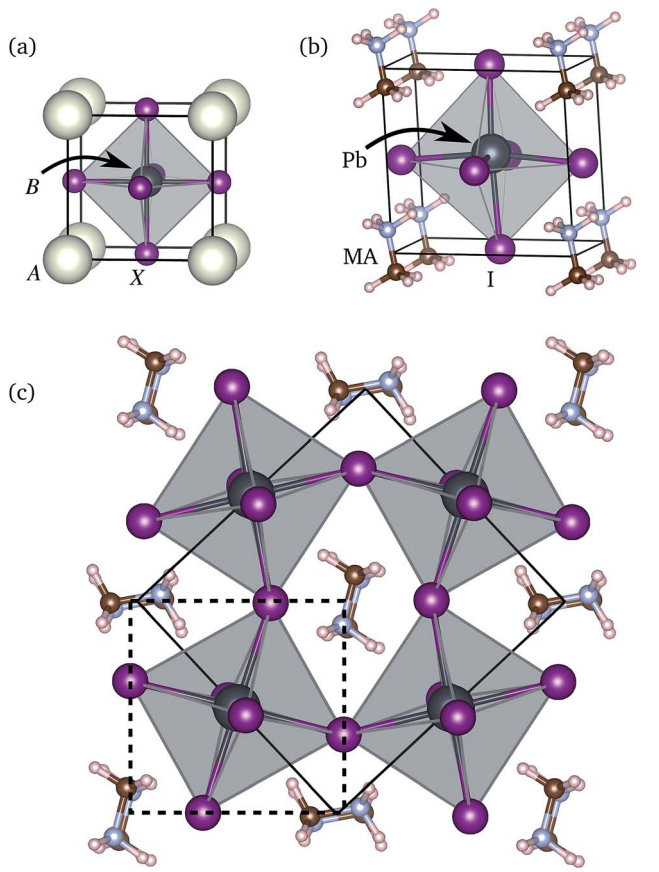

Fig. 2 (a) Crystal structure of the ideal ABX_3 perovskite ($Z = 1$), with the 12-fold coordinated A site and the octahedral B site, and a distorted $MAPbI_3$ perovskite (b) in the "α" ($Z = 1$, "3D") and (c) in the *Pnma* phase ($Z = 4$, "3D–OR"). The unit cell is marked by a solid black line; the dashed line surrounds a volume containing one formula unit.

2.2 Determining thermodynamic stability

For each considered ABX_3 composition, we first determine the formation energies of the perovskite crystal structure of $MAPbI_3$, more precisely the high-temperature tetragonal α phase (space group no. 99, *P4mm*) with one perovskite formula unit per unit cell ($Z = 1$)[36] (see Fig. 2(b)). The reason why we choose this specific crystal structure is because it is the one with the smallest possible unit cell. Its tetragonal symmetry is however only a macroscopic average over disordered hydrogen positions: the symmetry is locally broken in each unit cell and hence in our calculation as well. We observe that different configurations of the organic molecule lead to very small energy differences, which we can safely neglect at this stage of the investigation. Starting from the α (3D) phase, we replace methylammonium (MA) with H_3S, NH_4, MS, MP, FA, EA, G, AA, ED, or *t*BA, and we substitute F, Cl, or Br for I, and an element marked by the color orange in Fig. 1 for Pb. Here we chose typically divalent elements (group IIA, group IIB, group IV, and period-4 transition metals starting from Cr) and added a few more elements belonging to the neighboring rows or columns. All considered B elements have been observed in the divalent state according to ref. 37. For every composition we optimize the cell parameters and the atomic positions with DFT as implemented in the Vienna *Ab initio* Simulation Package VASP.[38]

More specifically, we use the generalized-gradient approximation of Perdew, Burke and Ernzerhof[39] (PBE) for the exchange–correlation functional, the projector-augmented wave (PAW) method with a basis of plane waves up to 520 eV, and Γ-centered Monkhorst–Pack *k*-point meshes with an approximately constant *k*-point density of about 500 *k*-points per $Å^{-3}$, which corresponds to $10 \times 10 \times 10$ *k*-point meshes for a simple cubic cell with a lattice parameter of 5 Å. All calculations include spin-polarization. The PAW setups are taken from VASP version 5.3. We note that it was found that the use of a van-der-Waals corrected functional does not lead to strong changes in the formation enthalpies of the considered phases (*i.e.*, small compared to the 10 meV per atom that we chose as the stability threshold).[4]

For the resulting geometry, the next step is the calculation of the distance from the crystal phase to the convex hull of thermodynamic stability. We recall that the convex hull is a hypersurface in composition space that connects all materials that are thermodynamically stable, *i.e.*, that have an energy lower than all possible decomposition channels (see also the ESI†).

For compounds close to thermodynamic stability (within 100 meV per atom), we also consider the orthorhombic (*Pnma*) low-temperature perovskite phase of $MAPbI_3$, which has a unit cell containing four perovskite formula units ($Z = 4$). This cell [see Fig. 2(c)] accommodates nonspherical ions, such as MA or FA, by octahedral rotation. To this set of compounds we also give the possibility to adopt one of several alternative (prototype) crystal structures. This is important, as many stoichiometries can crystallize in competing crystal phases, which can have very different properties as compared to perovskites. In fact, we will see that especially for larger A molecules the three-dimensional network of octahedra, which is characteristic of the perovskite structure, is no longer favored, while a lower-dimensional network of interconnected octahedra (1D and 2D) becomes more stable, leading unfortunately to a significant increase in the band gap.[40] To detect cases where this happens, we include a prototype for each network pattern of the octahedral networks (3D, 2D, and 1D). It is meaningful to test only a prototype per network type as we have verified that different structures with similar patterns lead to similar formation energies. The structure of $GGeI_3$ (the prototype with a 1D network of octahedra) was retrieved from the experimental study of Stoumpos *et al.* of germanium iodide perovskites,[7] while all other prototypes come from the Materials Project database.[41]

In ref. 15 the Goldschmidt Tolerance Factor (GTF) (a geometrical criterion based on ionic radii) was identified as a crucial parameter that decides which crystal structure is adopted. We note that to be as general as possible in our analysis, our prototypes also include one structure with a very small GTF ($\ll 1$) and one with a very large GTF ($\gg 1$), knowing that the perovskite structure is favored for a GTF close to 1. Moreover, experimental experience tells us that compounds with NH_4 as the A cation tend to form non-perovskite structures with edge-sharing octahedra. For this reason, we also include the NH_4CdCl_3 prototype (space group no. 62, *Pmnb*, that is also the ground-state structure of $CsPbI_3$).

Since the space group of the prototype is not always preserved when different molecules are inserted in the lattice, we use a label instead of space group names to denote structural characteristics. For example, the "*Pmna*" structure is a three-dimensional perovskite with octahedral rotations, which we

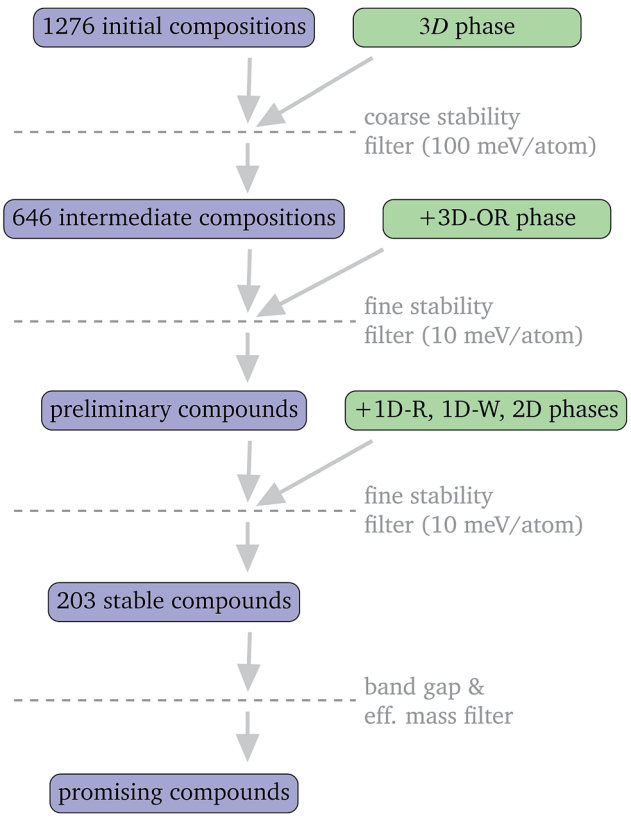

Fig. 3 High-throughput scheme.

label "3D–OR" in the following. In order to keep the computational cost of this study as low as possible, we used a smaller unit cell ($Z = 2$) for the "*Pnma*" phase, which contains the important octahedral rotation but in which the MA molecules are aligned in parallel, as opposed to the antiparallel alignment in the true *Pnma* phase of $MAPbI_3$. We have verified that the energy difference between the two structures of $MAPbI_3$ is negligible for our purposes (2 meV per atom). We would also like to note that the characteristics of the initial structure, such as octahedral rotations or deformations, might in some cases appear or disappear during structure optimization. We did not systematically investigate whether this is the case, but we did notice that as a consequence of symmetry removal, many of the initial "3D" perovskites distorted significantly during structural optimization.

The prototypes are listed in Table 1, and the prototype crystal structures are depicted in Fig. 4.

Once we have calculated the total energy of the different prototypes, the convex hull of stability is obtained using the quickhull algorithm of Barber and coworkers,[42] taking advantage of the reservoir compounds present in the Materials Project[41] database and in the Open Quantum Materials Database.[43] Temperature effects are neglected here, as their calculation would require to determine the phonon band structure of all compounds. We expect that vibrational and configurational entropies may be non-negligible at high temperatures and eventually affect the ordering of the different phases. However, we are interested in relative stability (energy differences) between $MAPbI_3$ and hybrid perovskites obtained by chemical substitution, where temperature effects are expected to be less important. We consider a compound to be thermodynamically stable if its distance from the convex hull is $\leq$10 meV per atom. With this criterion we find 203 stable compounds.

2.3 Calculation of band gaps

In order to assess the suitability of the stable candidates as photovoltaic absorbers and estimate the mobility of charge carriers, we calculate electronic band gaps and effective electron and hole masses.

To correct for the typical band gap underestimation by semi-local DFT, the band gaps of the stable candidates are calculated with the hybrid exchange–correlation functional of Heyd, Scuseria, and Ernzerhof[44] (HSE06), which contains 25% Hartree–Fock exchange. This functional yields an excellent agreement with experiment for materials with band gaps between 0.5 eV and 2.5 eV, which includes the range of interest for photovoltaic applications. In order to save computation time,

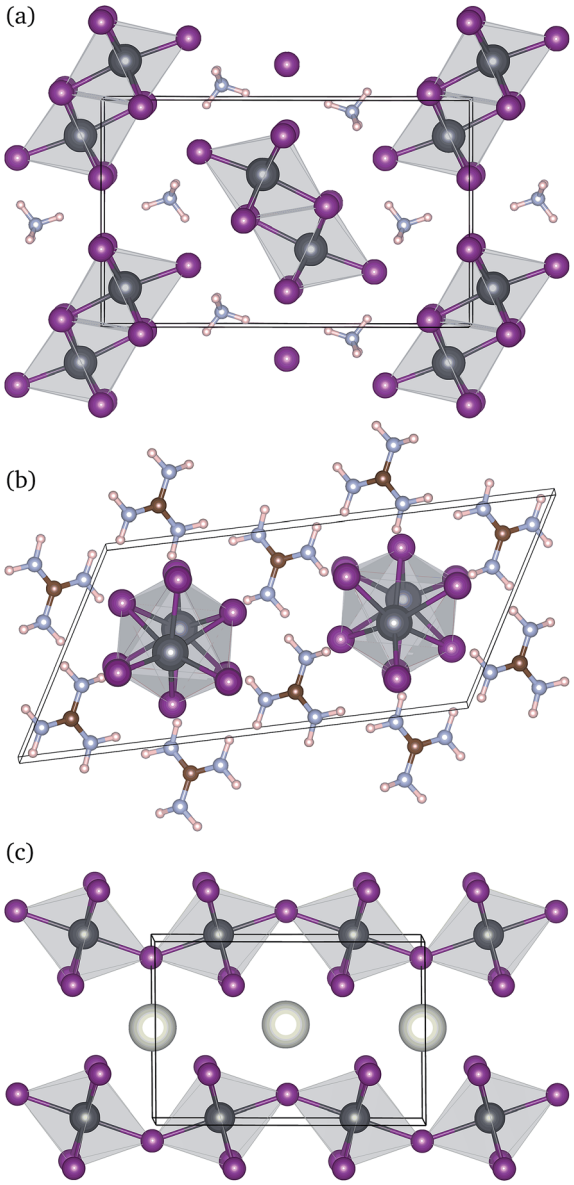

Fig. 4 Non-perovskite prototype crystal structures: (a) NH_4CdCl_3 (*Pmnb*, "1D–R"), (b) $GGeI_3$ ($P2_1/c$, "1D–W"), and (c) $CaIrO_3$ (*Cmcm*, "2D").

Table 1 Prototype crystal structures of ABX_3 compounds considered, space group number and symbol, number of formula units Z in the unit cell, and connection of neighboring octahedra (corner-sharing CS as in perovskites, or edge-sharing ES, or face-sharing FS), dimensions of the octahedral network (1D, 2D, or 3D), and our label based on octahedron properties (OR = octahedral rotation, W = wire, and R = ribbon)

Prototype	Space group	Z	Octahedra	Network	Label
NH_4CdCl_3	62 (*Pmnb*)	4	ES	1D	1D–R
$GGeI_3$	14 ($P2_1/c$)	4	FS	1D	1D–W
$CaIrO_3$	63 (*Cmcm*)	2	ES, CS	2D	2D
Perovskite	1 ($P1$)	1	CS	3D	3D
Perovskite	62 (*Pnma*)	4	CS	3D	3D–OR

Table 2 Comparison of band gaps with and without SOC from PBE and HSE for $CsPbI_3$ and $CsSnI_3$ in eV

	E_g of $CsPbI_3$			E_g of $CsSnI_3$		
	w/o SOC	w SOC	SOC	w/o SOC	w SOC	SOC
PBE	1.48	0.27	−1.21	0.44	0.05	−0.39
HSE	2.01	0.68	−1.34	0.82	0.40	−0.43

band gaps from HSE are only calculated for materials with a PBE band gap ≤ 2.0 eV (materials potentially suitable as photovoltaic absorbers). We also reduce the *k*-point density to about 60 *k*-points per Å^{-3}, which corresponds to a 5 × 5 × 5 *k*-point mesh for a simple cubic cell with an edge length of 5 Å.

For compounds for which we calculated HSE gaps, we include spin–orbit coupling (SOC) at the PBE level and use the resulting SOC correction to the band gap also in the HSE calculations in order to avoid computationally expensive HSE + SOC calculations. We have verified for cubic $CsPbI_3$ and $CsSnI_3$ that the PBE and the HSE functional yield similar SOC energies (about 10% difference) in spite of quite different band gaps (see Table 2). For semiconductors with a vanishing PBE bandgap, we use the SOC from a PBE + *U* calculation if PBE + *U* opens the gap. We employ a Hubbard-*U* for d orbitals identical to those used in the Materials Project.[41] Additionally, we use a Hubbard-*U* of 1 eV for d orbitals of Cu, Au, and Ag. In the few cases where we

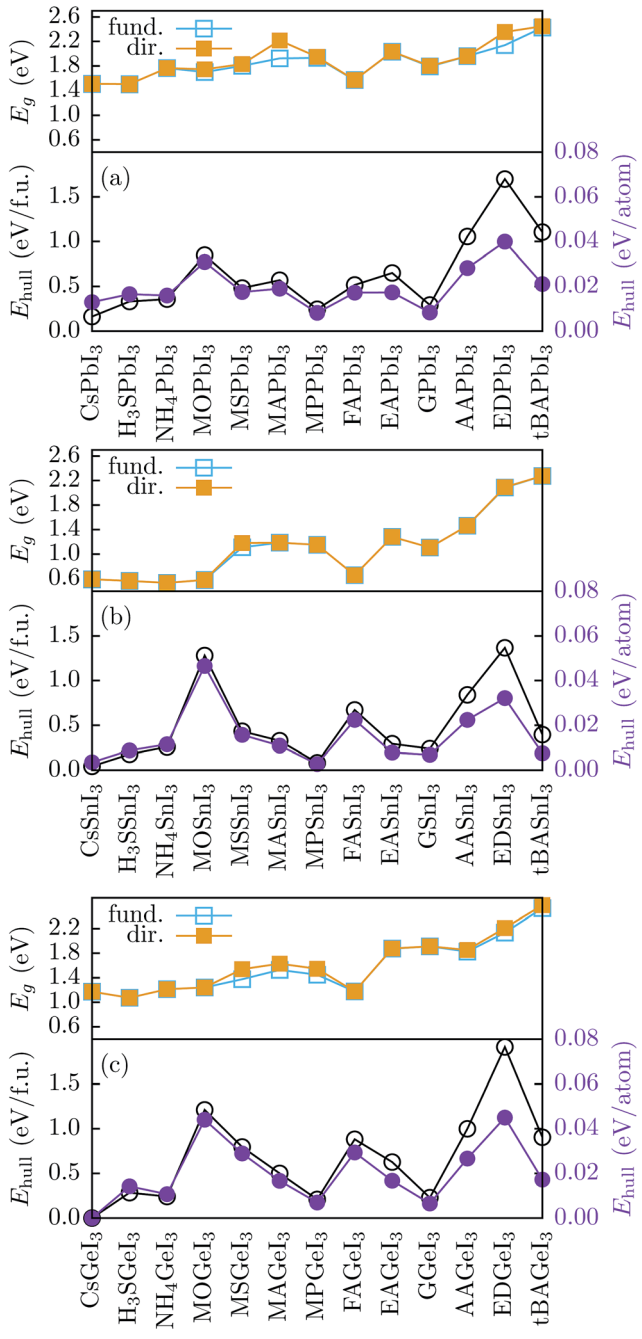

Fig. 5 (a) Distance from the convex hull of stability, E_{hull}, and fundamental and direct PBE band gaps of $APbI_3$ with different A cations; (b) and (c) the same as (a) with Sn and Ge, respectively, instead of Pb. Besides the molecules shown in Fig. 1, here we also considered the element Cs and the molecule methyloxonium (CH_3OH_2, MO).

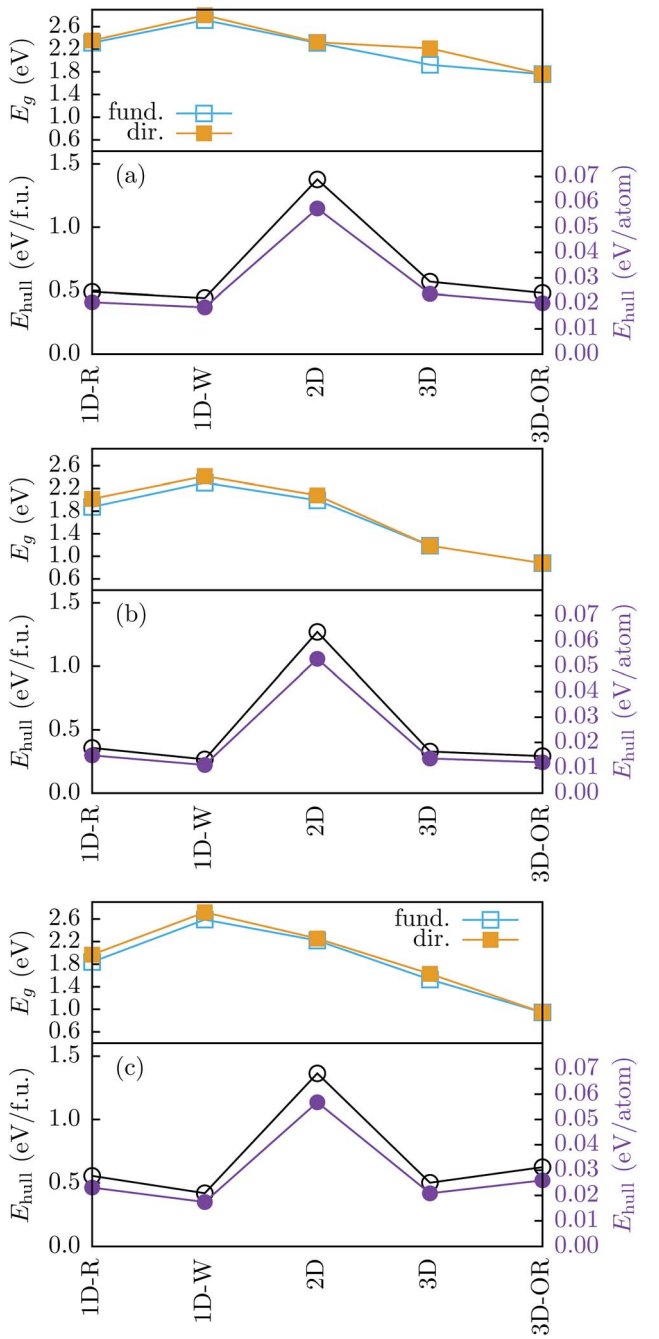

Fig. 6 (a) Distance from the convex hull of stability, E_{hull}, and fundamental and direct PBE band gaps of $MAPbI_3$ with different crystal structures; (b) and (c) the same as (a) with Sn and Ge, respectively, instead of Pb.

happened to calculate the band gap including SOC from HSE, we use directly that value.

2.4 Calculation of effective masses

The effective mass tensors $\underline{\underline{M}}$ are calculated at the PBE level with the program BoltzTraP[45] as

$$\left\langle \left(M^{-1}\right)_{\alpha\beta} \right\rangle = \frac{\sum_n \int \mathrm{d}\boldsymbol{k} \frac{\partial^2 \varepsilon_{n\boldsymbol{k}}}{\partial k_\alpha \partial k_\beta} f_{n\boldsymbol{k}}}{\sum_n \int \mathrm{d}\boldsymbol{k} f_{n\boldsymbol{k}}}, \quad (1)$$

where n is the band index, the energy eigenvalues $\varepsilon_{n\boldsymbol{k}}$ are taken from a Fourier-interpolated band structure, and $f_{n\boldsymbol{k}}$ is the Fermi distribution. This quantity depends on temperature and the chemical potential μ, which is adjusted by the doping level. We assume ambient temperature (300 K) and a doping level of 10^{18} cm^{-3}. The inverse mass tensors are afterwards inverted, and their eigenvalues averaged over the three directions. For semiconductors with a vanishing PBE bandgap, we use the effective masses from a PBE + U calculation if PBE + U opens the gap. If this does not occur, we omit the effective mass. We do not calculate effective masses at the HSE level, as we would not be able to converge the effective masses with respect to the number of k-points. Our effective mass m^* is the reduced mass, $m^* = 1/(1/m_e^* + 1/m_h^*)$. In this way, we identify materials which are both good electron and hole conductors, like $MAPbI_3$.

3 Results and discussion

3.1 Stable phases and compositions

Starting from $MAPbI_3$, we can try to enhance stability by replacing MA by a different molecular ion. In Fig. 5 we compare the stability and band gap of $APbI_3$ in a simple 5-atom perovskite structure for different A cations. As we can see in the case of $APbI_3$, MA is not the molecule that yields the most stable crystalline compounds. When we apply our stability criterion, we see that both $MAPbI_3$ and $FAPbI_3$ are thermodynamically unstable. These findings are perfectly in line with the experimental observation that $MAPbI_3$ and $FAPbI_3$ are easily subject to light-induced degradation, especially in the presence of oxygen and moisture. Our results suggest that the substitution of MA by MP or G can enhance stability against decomposition. To a lesser extent, substitution by NH_4 or H_3S does the same. The other two group-IV compounds, $ASnI_3$ [Fig. 5(b)] and $AGeI_3$ [Fig. 5(c)], show a very similar behavior. Furthermore, we observe that, except for the very flat molecules FA and G, the band gap increases almost monotonically with molecule size. Next, we compare the dependence of the thermodynamic stability and band gap on the crystal structure for some $MABI_3$ compounds (B = Pb, Sn, and Ge) in Fig. 6. The trend is the same for all three B elements. The two perovskite structures, 3D and 3D–OR, are almost at the same energy, and also the two 1D structures are very similar in energy compared to each other and compared to the 3D prototypes. The 2D structure is very unstable for these compositions. The 3D and 3D–OR structures possess the smallest band gaps. In Fig. 7, we show the frequency of occurrence of the elements and molecules in the stable compounds (compounds within a threshold of 10 meV per atom above the convex hull of stability). We see that the most suitable molecules (the ones that form the largest number of stable compounds) are NH_4, MP, and H_3S. G, MS, *t*BA, and EA appear less often. MA, FA, AA, and ED do not form any stable compound.

On the B site, we find mainly the group-IV elements Sn, Ge, and Pb, but also group-II elements (Ca, Sr, Be, Mg, and Ba) and IIB elements (Zn, Cd, and Hg) are not scarce. There are also a few compounds with IIIA elements (In and Tl) and IA elements (Au, Ag, and Cu), and some with other transition metals (Mn, Fe, Co, and Pd). We also find Te and Se a few times. On the halide site, we find mainly Br and Cl, but there are also about 40 iodides and a few fluorides.

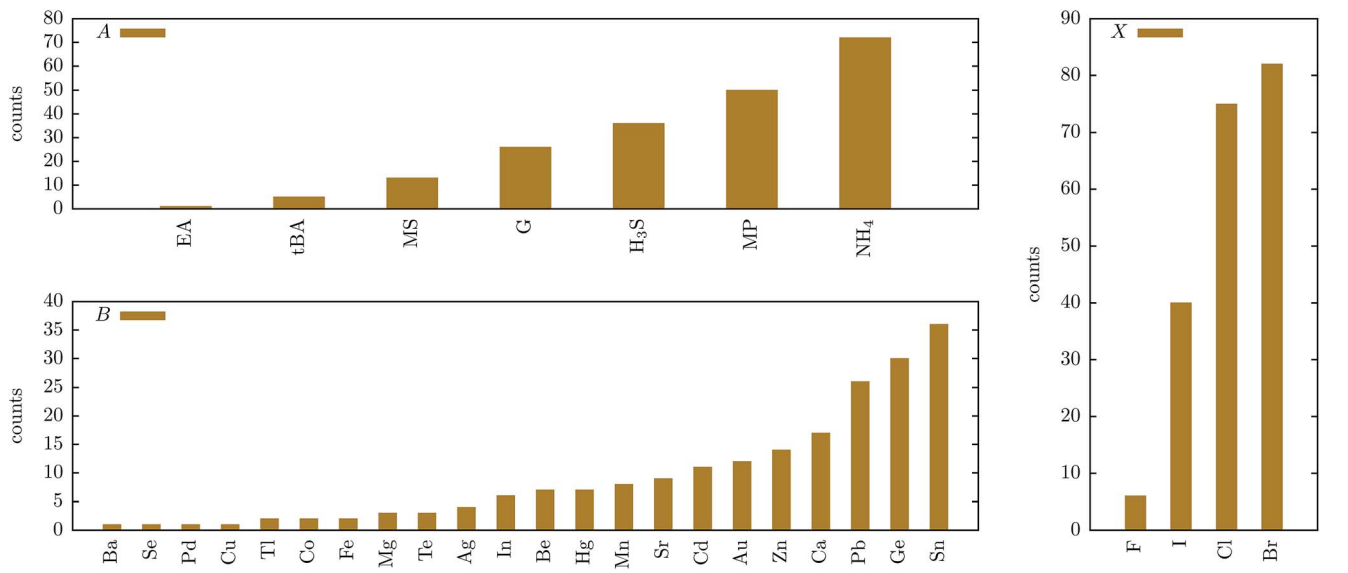

Fig. 7 Frequency of occurrence of the elements and molecules in the stable compounds.

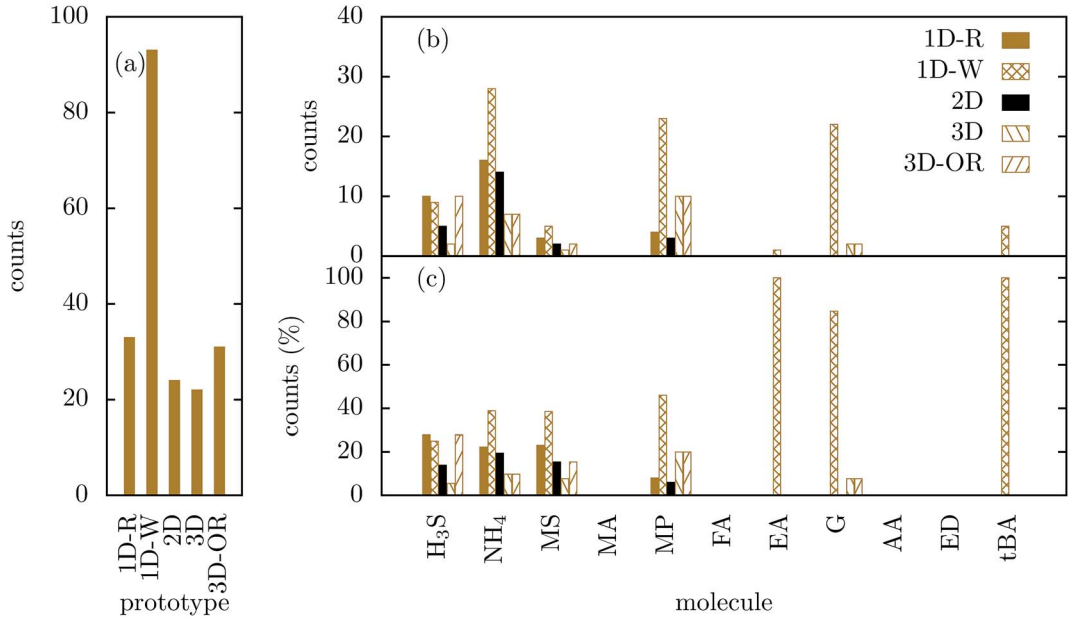

Fig. 8 (a) Frequency of occurrence of the considered prototype crystal structures in the stable compounds; (b) the same as (a) for each molecule separately; and (c) the same as (b) in %.

We find that many compounds favor crystallization in one of the (distorted) prototype structures with several formula units per unit cell (see Table 1 for definitions). In Fig. 8(a) we show the frequency of occurrence of the prototype crystal structures over the stable compounds. The most common crystal structure is the 1D–W structure with about 90 counts, and the other prototypes appear about 20–30 times. The prevalence of phases other than the simple perovskite phase is not surprising considering that most of the molecules are highly non-spherical and strongly distort the perovskite unit cell from its ideal cubic shape (see Fig. 2). The same happens for $MAPbI_3$, whose lowest-energy structure at zero temperature is a larger orthorhombic unit cell with *Pnma* symmetry (see Fig. 2(c)), where the orientation of neighboring organic molecules alternates in combination with octahedral rotation. In Fig. 8(b) and (c) we show the distribution of the prototype crystal structures, separately for each molecule, once in absolute numbers [Fig. 8(b)] and once in % [Fig. 8(c)]. The molecules are approximately sorted by size, from small (H_3S) to large (*t*BA). The 1D–R, 2D, 3D, and 3D–OR structures occur only in combination with smaller molecules, while the 1D–W structure forms stable compounds with molecules of all sizes.

3.2 Band gaps

Of the total 203 stable ABX_3 compounds (see the ESI† for a complete list), only 12 compounds have a band gap suitable for photovoltaics. In Fig. 9, we show the average and maximum band gap of the stable compounds with a given prototype crystal structure. We see that the two perovskite structures, 3D and 3D–

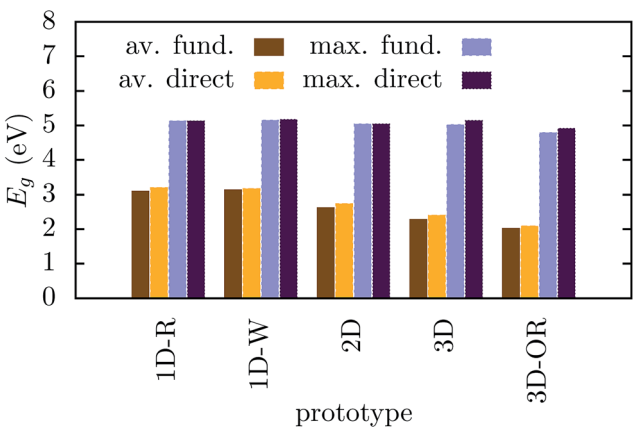

Fig. 9 Averaged and maximum fundamental and direct band gaps E_g of the compounds as a function of the prototype crystal structure, calculated at the PBE level. All minimum band gaps are zero.

Table 3 Calculated HSE band gaps (including SOC), effective mass m^*, and distance from the convex hull of stability E_{hull} in eV per atom of ABX_3 compounds with gaps interesting for photovoltaics

	HSE gap			
Composition	Fund.	Direct	m^*	E_{hull}
NH_4AuI_3–1D–W	1.26	1.30	10.15	0.000
NH_4AuBr_3–1D–W	1.70	1.70	13.63	0.001
NH_4AuBr_3–2D	1.22	1.31	6.54	0.002
NH_4AuI_3–2D	1.00	1.10	1.35	0.002
H_3SSnBr_3–3D–OR	1.67	1.67	0.22	0.004
NH_4AuCl_3–2D	1.53	1.56	2.29	0.005
$MSAuBr_3$–1D–W	1.23	1.24	315.48	0.005
$MPSnI_3$–3D–OR	1.18	1.18	0.16	0.005
$MPSnI_3$	1.35	1.35	0.52	0.007
NH_4AgCl_3–2D	1.31	1.44	1.61	0.008
$MSSeBr_3$–3D–OR	1.54	1.55	26.86	0.008
$MSTeBr_3$–1D–R	1.53	1.55	54.27	0.010

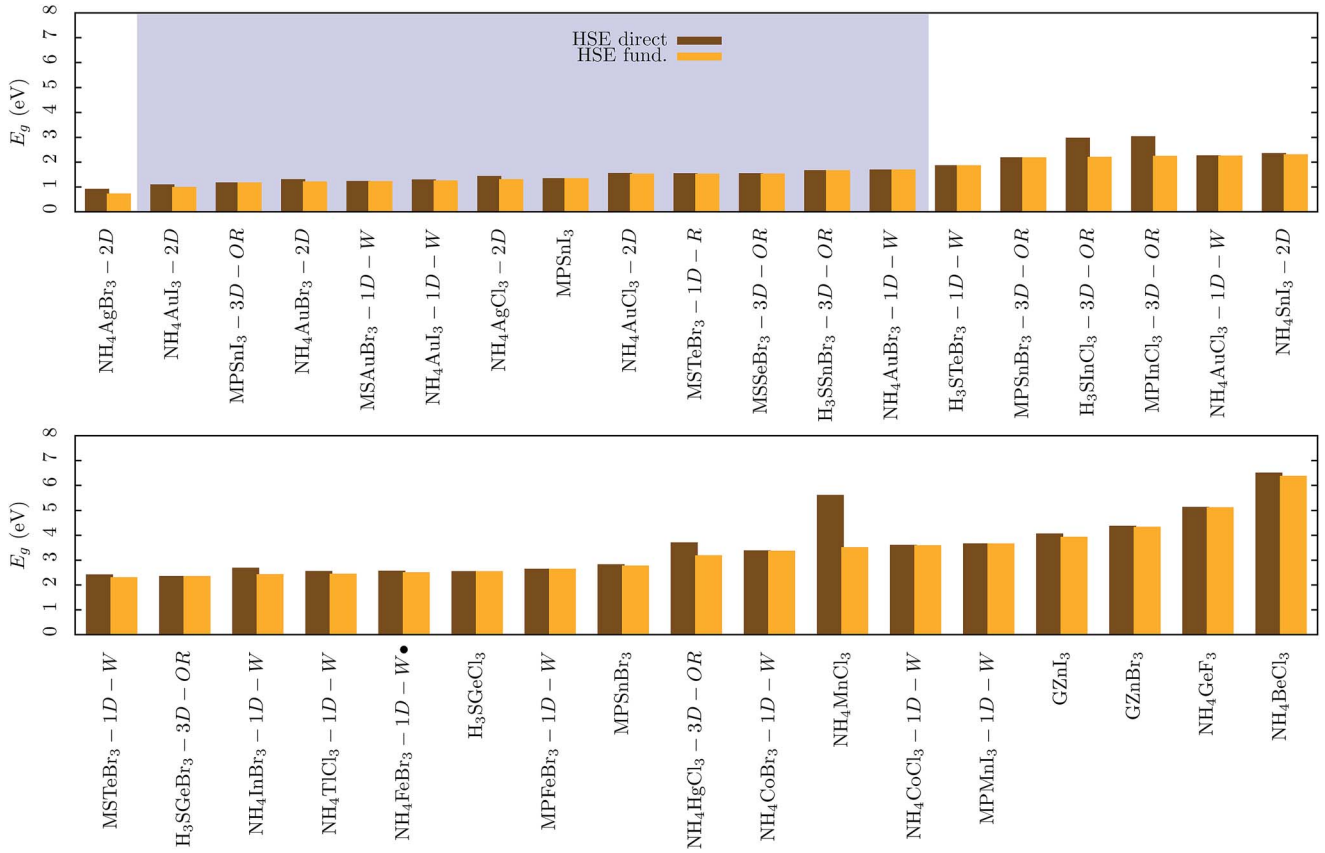

Fig. 10 Band gaps E_g of the compounds (where E_g > 0.5 eV), sorted by size. Compositions already listed in the databases are marked by a ●.

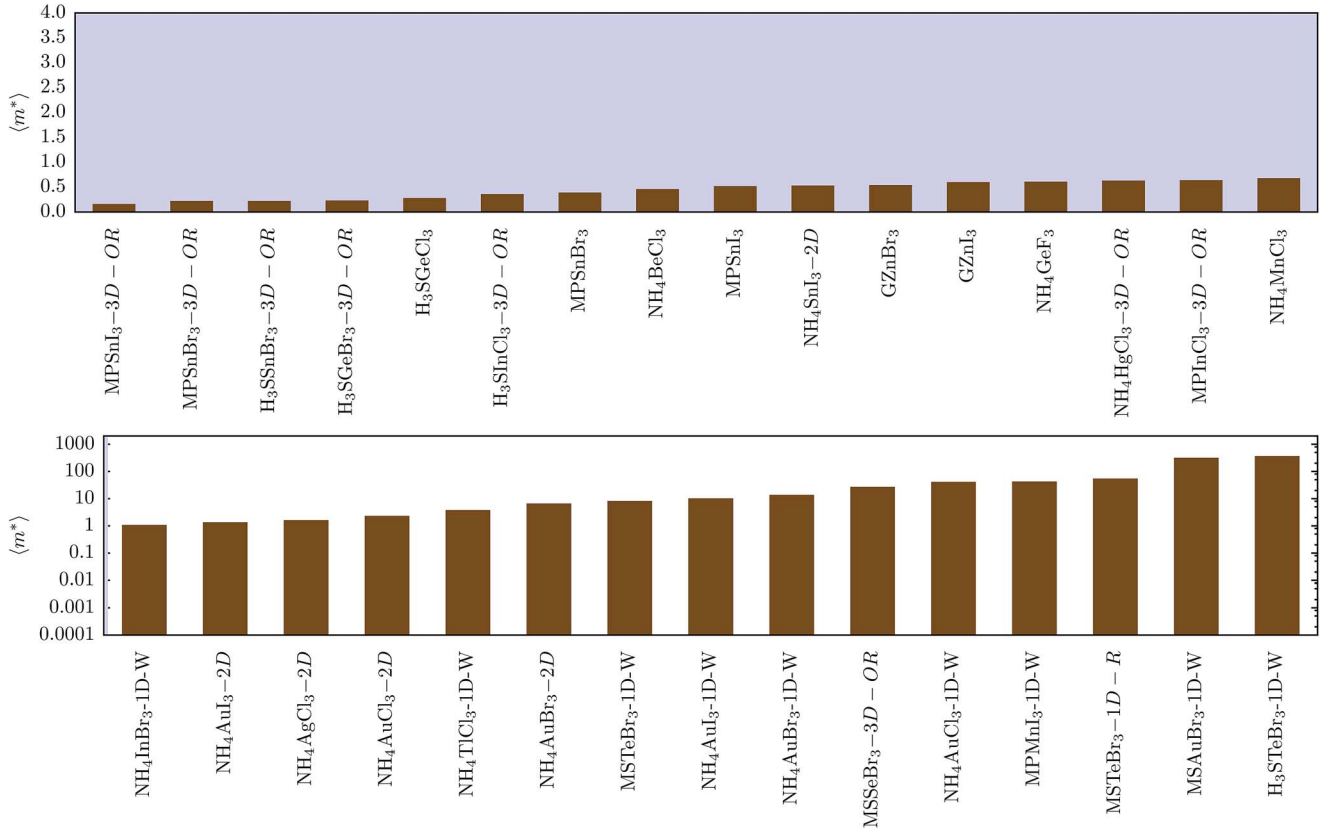

Fig. 11 Effective masses m^* of the compounds, averaged over electrons and holes and sorted by size.

Table 4 Calculated HSE band gaps, effective mass m^*, and distance from the convex hull of stability E_{hull} in eV per atom of ABX_3 compounds with small effective masses

	HSE gap					
Composition	Fund.	Direct	m^*	m_e^*	m_h^*	E_{hull}
$MPSnBr_3$–3D–OR	2.19	2.19	0.22	0.58	0.35	0.000
$GZnBr_3$	4.34	4.38	0.54	0.55	25.10	0.000
$MPSnBr_3$	2.78	2.83	0.39	1.03	0.63	0.001
H_3SInCl_3–3D–OR	2.21	2.98	0.36	0.74	0.69	0.001
$MPInCl_3$–3D–OR	2.25	3.04	0.64	0.87	2.41	0.001
H_3SGeBr_3–3D–OR	2.36	2.36	0.23	0.58	0.37	0.003
H_3SSnBr_3–3D–OR	1.67	1.67	0.22	0.77	0.30	0.004
H_3SGeCl_3	2.55	2.55	0.28	1.07	0.37	0.005
$MPSnI_3$–3D–OR	1.18	1.18	0.16	0.64	0.22	0.005
$MPSnI_3$	1.35	1.35	0.52	0.89	1.23	0.007
NH_4HgCl_3–3D–OR	3.19	3.71	0.63	0.75	4.11	0.007
NH_4MnCl_3	3.52	5.61	0.68	2.03	1.03	0.008
NH_4SnI_3–2D	2.31	2.36	0.53	2.59	0.67	0.008
NH_4GeF_3	5.13	5.14	0.61	1.33	1.11	0.009
NH_4BeCl_3	6.38	6.51	0.46	0.51	4.93	0.010
$GZnI_3$	3.94	4.07	0.60	0.65	7.61	0.010

OR, have the smallest average band gap. We compiled all candidates with band gaps interesting for photovoltaics in Table 3. We find that all types of octahedral networks (1D–R, 1D–W, 2D, 3D, and 3D–OR) are present in this group. A summary of the results concerning the size of the band gaps is depicted in Fig. 10. Gaps in the range interesting for photovoltaics (0.75 eV to 1.75 eV) are shaded in blue. We find that most (7) compounds with suitable band gaps have a group-IA element on the B site (Au and Ag). As expected, we find Sn-based compounds, but also one each containing Se or Te. As for the molecules, only NH_4, MS, MP, and H_3S show up. Apart from two chlorides, we find mainly bromides (6) and iodides (4) here, as the lighter halogens tend to increase the band gap. We note again that some experimentally known compounds with similar band gaps do not appear here because they are not stable enough to satisfy our stability criterion (*e.g.*, $MAPbI_3$ and $FAPbI_3$).

3.3 Effective masses

In Fig. 11, we show the reduced effective masses of the same compounds. The region of small effective masses (up to one electron mass) is shaded in blue. The 16 compounds with small effective masses are also compiled in Table 4. We find that many (9) compounds have group-IV elements on the B site (Sn and Ge), but there are also a few compounds with In, Zn, Hg, Mn, or Be on the B site. Most compounds (all but one) with low effective masses have 3D octahedral networks. The only non-3D compound with a small m^* is NH_4SnI_3–2D. We note that at a given composition, this 3D network tends to yield the lowest effective mass. The separate effective masses of electrons and holes, m_e^* and m_h^*, are depicted in Fig. 12 and 13. We see that there are 11 compounds with small m_e^*, but only 8 with small m_h^*, and 16 with a small

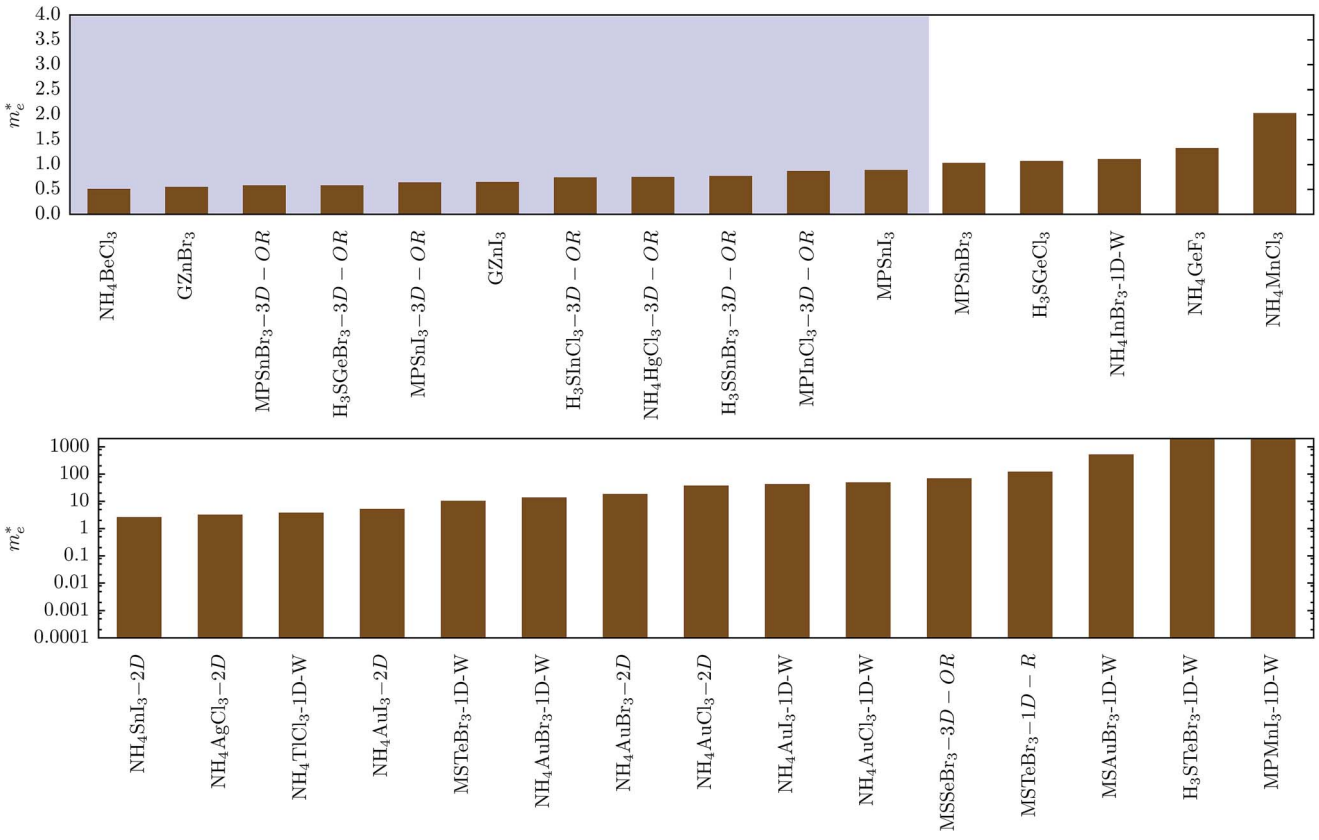

Fig. 12 Effective electron masses m_e^* of the compounds, sorted by size.

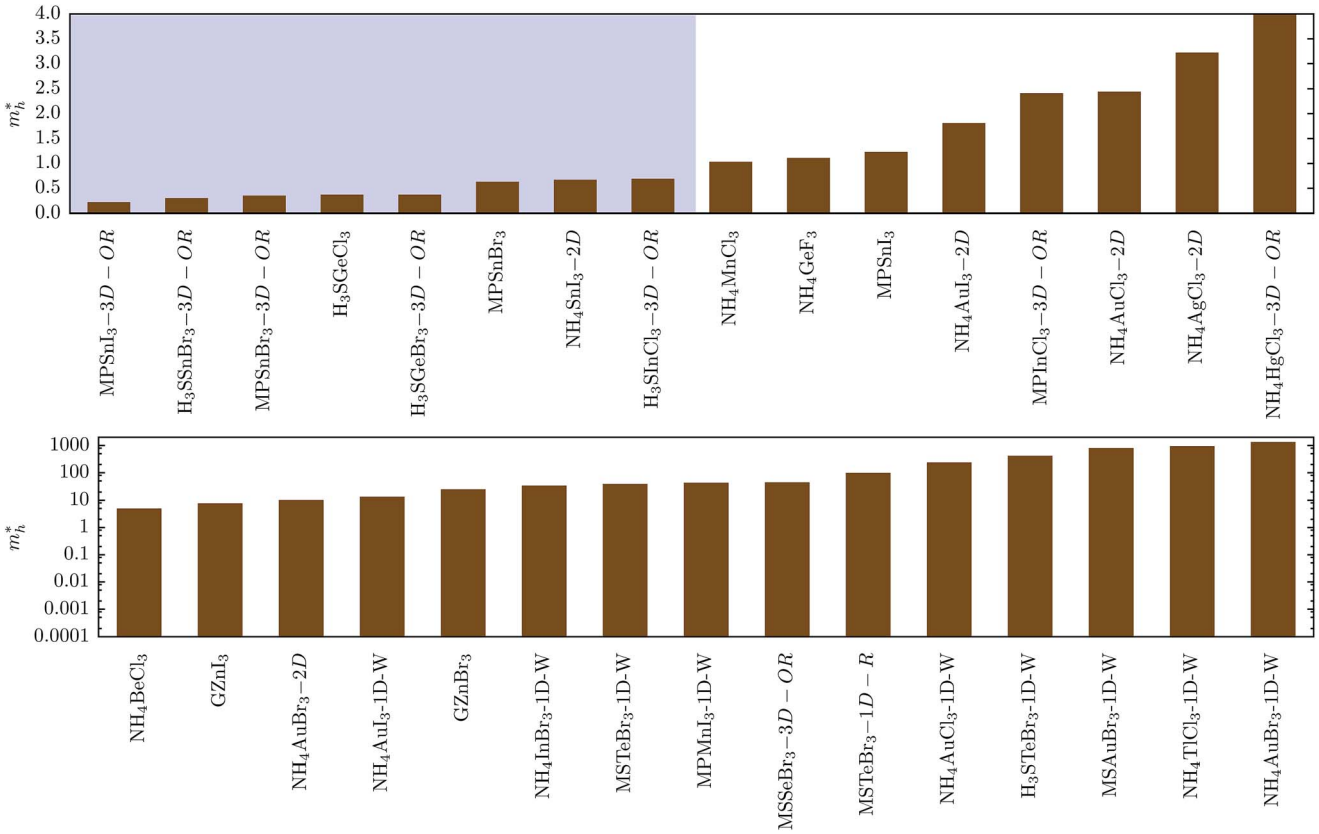

Fig. 13 Effective hole masses m_h^* of the compounds, sorted by size.

Table 5 Comparison of our calculations with available experimental data

Compound	Property	Calculation	Experiment
$GGeI_3$	Direct E_g	2.91 eV	2.7 eV (ref. 7)
$MAGeI_3$	Direct E_g	1.92 eV	1.9 eV (ref. 7)
$MAPbI_3$	Direct E_g	1.82 eV	1.61–1.65 eV (ref. 46)
$MAPbI_3$	Reduced eff. mass	$0.233m_0$	$0.104m_0$ (ref. 46)

reduced mass m^*. While the group of compounds with small m_h^* consists almost only of group-IV (Sn and Ge) halides (apart from one In compound), the group of compounds with small m_e^* is more heterogeneous and contains also Zn, In, Be, and Hg halides.

3.4 Comparison with experiment

In order to judge the predictivity of our calculations, in Table 5 we compare some properties with available experimental data.

We can see that the agreement with experiment is fully satisfactory. We hope that our predictions will now motivate further experiments on the most promising compounds that we have identified.

3.5 Comparison with theory

Compared to the computational studies of El-Mellouhi[31] and Jiang,[33] we confirm the stabilizing effect of replacing MA by H_3S or MP, but in contrast to El-Mellouhi, we do not find that MS improves stability. While Jiang found $MAZnI_3$, $MACdI_3$, and $MABeI_3$ to be stable, we do not, which may be explained by the fact that we include more decomposition channels than Jiang. We do find similar direct band gaps of 3.58 eV for $MAZnI_3$ and of 1.36 eV for $MACdI_3$ to those of Jiang (3.76 and 1.27 eV); however our band gap of 3.81 eV for $MABeI_3$ differs strongly from that of Jiang (0.92), which is probably caused by Jiang and us considering different metastable structures of $MABeI_3$.

3.6 Lead halides

The stable compositions with band gaps interesting for photovoltaics are all lead-free. In Table 6 we list Pb halides with favorable band gaps. These compounds are metastable, but in some cases still more stable than $MAPbI_3$. In the cases of metastable compounds where we did not perform a HSE calculation, we estimate the band gap using a linear fit (details are given in the ESI†).

4 Summary and conclusions

We screened a large part of the periodic table for possible substitutions for Pb, MA, and I in $MAPbI_3$ that may enhance the thermodynamic stability of hybrid organic–inorganic perovskites. It turns out that there are a few elements that may help

Table 6 Calculated HSE band gaps (including SOC), estimated direct gaps ("est. dir."), effective mass m^*, and distance from the convex hull of stability E_{hull} in eV per atom of $APbX_3$ compounds with estimated gaps interesting for photovoltaics. Compositions already listed in the databases are marked by a •

	HSE gap				
Composition	Fund.	Dir.	Est. dir.	m^*	E_{hull}
$MPPbI_3$–3D–OR	1.20	1.20	1.45	0.22	0.017
$MPPbI_3$	2.76	2.75	1.68	0.82	0.020
$GPbI_3$	1.27	1.26	1.51	0.33	0.021
H_3SPbBr_3			1.58	0.22	0.024
H_3SPbI_3–3D–OR			1.39	0.37	0.031
NH_4PbI_3•			1.47	0.29	0.040
$MAPbI_3$–3D–OR•			1.46	0.24	0.040
H_3SPbI_3			1.17	0.27	0.041
$MAPbI_3$–3D–OR•			1.57	0.30	0.042
$EAPbI_3$–3D–OR			1.57	0.27	0.042
$MSPbI_3$			1.55	0.56	0.044
$MAPbI_3$–β•			1.50	0.26	0.046
$FAPbI_3$–3D–OR•			1.34	0.16	0.047
NH_4PbI_3–3D•			1.11	0.15	0.047
$MAPbI_3$–3D•			1.54	0.26	0.047
$MSPbI_3$–3D–OR			1.46	0.25	0.048
$FAPbI_3$•			1.25	0.17	0.059
$AAPbI_3$–3D–OR			1.65	0.37	0.061
$AAPbI_3$			1.69	0.81	0.070
$MSPbI_3$–2D			1.68	9.49	0.117
$MOPbI_3$			1.45	0.49	0.119
tBA$PbCl_3$–3D–OR			1.48	5.89	0.123
$FAPbI_3$–2D•			1.59	3.22	0.234
$GPbI_3$–3D–OR			1.42	1.91	0.283

stabilize hybrid perovskites if substituted partly for Pb. We also find that the A site ion can be used to improve stability. In fact, MA substitution is probably the most promising strategy to improve the thermodynamic stability of $MAPbI_3$. Ammonium (NH_4), methyl phosphonium (CH_3–PH_3, MP), sulfonium (H_3S), guanidinium [$C(NH_2)_3$, G], and methyl sulfonium (CH_3–SH_2, MS) can enhance the stability of the material compared to MA, meaning that there are more stable compounds with these molecules on the A site than with methylammonium (MA). Especially promising are compounds with methyl phosphonium or H_3S as the molecular cation and a group-IV element on the B site, since these compounds combine a favorable band gap with a small effective mass. Compounds with group-IA elements (Ag or Au) or group-VI (Se and Te) on the Pb site can yield similarly suitable band gaps of 1–2 eV. These latter compounds deserve more attention, although they tend to have larger effective masses. We also see that the effective mass can depend strongly on the crystal phase, as in the case of $MPSnI_3$, where we find $m^* = 0.16$ for the 3D–OR phase, but a much larger value of $m^* = 0.52$ for the distorted perovskite. We find candidates with small effective electron masses among both the group-IV (Ge, Sn, and Pb) halides and transition-metal (Zn and Hg) and other (Be and In) compounds, but mainly the group-IV halides have simultaneously both small effective hole and electron masses. Our unbiased high-throughput approach is in principle capable of yielding unexpected compounds. However, here we find that after having searched a vast composition space systematically, the most promising compounds for photovoltaics identified by this work are $MPSnI_3$ and H_3SSnBr_3. Note that $MPSnI_3$ has a smaller band gap than the reference compound $MAPbI_3$, indicating more efficient light harvesting. Another strategy to stabilize $MAPbI_3$ could be to replace Pb only partially by group-II elements such as Ba, Sr, or Ca, or Cd, in order to stabilize the compound. Since these elements increase the band gap, their fraction in a solid solution should however be kept small in order to avoid a loss in solar power conversion efficiency.

Conflicts of interest

There are no conflicts of interest to declare.

Acknowledgements

Crystal structures were visualized with VESTA,[47] and gnuplot and python-matplotlib were used for the other graphs. M. A. L. M. acknowledges partial support from the DFG through projects SFB-762 and MA-6786/1. Computational resources were provided by the Leibniz Supercomputing Centre through the SuperMUC projects p1841a and pr48je. S. K. thanks Carlo Motta for helpful discussion.

References

1 National Renewable Energy Laboratory (NREL), Best Research-Cell Efficiencies, http://www.nrel.gov/ncpv/images/efficiency_chart.jpg, 2015.
2 A. Kojima, K. Teshima, Y. Shirai and T. Miyasaka, *J. Am. Chem. Soc.*, 2009, **131**, 6050–6051.
3 G. Niu, X. Guo and L. Wang, *J. Mater. Chem. A*, 2015, **3**, 8970–8980.
4 Y.-Y. Zhang, S. Chen, P. Xu, H. Xiang, X.-G. Gong, A. Walsh and S.-H. Wei, *AIP Adv.*, 2015, 01301.
5 S. D. Stranks and H. J. Snaith, *Nat. Nanotechnol.*, 2015, **10**, 391–402.
6 K. P. Marshall, R. I. Walton and R. A. Hatton, *J. Mat. Chem. A*, 2015, **3**, 11631–11640.
7 C. C. Stoumpos, L. Frazer, D. J. Clark, Y. S. Kim, S. H. Rhim, A. J. Freeman, J. B. Ketterson, J. I. Jang and M. G. Kanatzidis, *J. Am. Chem. Soc.*, 2015, **137**, 6804–6819.
8 N. Pellet, P. Gao, G. Gregori, T.-Y. Yang, M. K. Nazeeruddin, J. Maier and M. Grätzel, *Angew. Chem., Int. Ed.*, 2014, **53**, 3151–3157.
9 M. Saliba, T. Matsui, J.-Y. Seo, K. Domanski, J.-P. Correa-Baena, M. K. Nazeeruddin, S. M. Zakeeruddin, W. Tress, A. Abate, A. Hagfeldt, *et al.*, *Energy Environ. Sci.*, 2016, **9**, 1989–1997.
10 Y. Wang, T. Zhang, G. Li, F. Xu, T. Wang, Y. Li, Y. Yang and Y. Zhao, *J. Energy Chem.*, 2018, **27**, 215–218.
11 J. H. Noh, S. H. Im, J. H. Heo, T. N. Mandal and S. I. Seok, *Nano Lett.*, 2013, **13**, 1764–1769.

12 Q. Tai, P. You, H. Sang, Z. Liu, C. Hu, H. L. Chan and F. Yan, *Nat. Commun.*, 2016, **7**, 11105.
13 J. Chen, Y. Rong, A. Mei, Y. Xiong, T. Liu, Y. Sheng, P. Jiang, L. Hong, Y. Guan, X. Zhu, *et al.*, *Adv. Energy Mater.*, 2016, **6**, 1502009.
14 J.-W. Lee, D.-H. Kim, H.-S. Kim, S.-W. Seo, S. M. Cho and N.-G. Park, *Adv. Energy Mater.*, 2015, **5**, 1501310.
15 Z. Li, M. Yang, J.-S. Park, S.-H. Wei, J. Berry and K. Zhu, *Chem. Mater.*, 2016, **28**, 284–292.
16 D. P. McMeekin, G. Sadoughi, W. Rehman, G. E. Eperon, M. Saliba, M. T. Hörantner, A. Haghighirad, N. Sakai, L. Korte, B. Rech, *et al.*, *Science*, 2016, **351**, 151–155.
17 I. E. Castelli, T. Olsen, S. Datta, D. D. Landis, S. Dahl, K. S. Thygesen and K. W. Jacobsen, *Energy Environ. Sci.*, 2012, **5**, 5814–5819.
18 R. Sarmiento-Perez, T. F. T. Cerqueira, S. Körbel, S. Botti and M. A. L. Marques, *Chem. Mater.*, 2015, **27**, 5957–5963.
19 S. Körbel, M. A. L. Marques and S. Botti, *J. Mater. Chem. C*, 2016, **4**, 3157–3167.
20 G. Ceder, *Mater. Res. Bull.*, 2010, **35**, 693–701.
21 X. Zhang, Y. Wang, J. Lv, C. Zhu, Q. Li, M. Zhang, Q. Li and Y. Ma, *J. Chem. Phys.*, 2013, **138**, 114101.
22 H. Katayama-Yoshida, K. Sato, H. Kizaki, H. Funashima, I. Hamada, T. Fukushima, V. Dinh and M. Toyoda, *Appl. Phys. A*, 2007, **89**, 19–27.
23 G. Hautier, A. Miglio, G. Ceder, G.-M. Rignanese and X. Gonze, *Nat. Commun.*, 2013, **4**, 2292.
24 T. F. Cerqueira, S. Lin, M. Amsler, S. Goedecker, S. Botti and M. A. Marques, *Chem. Mater.*, 2015, **27**, 4562–4573.
25 V. Sharma, C. Wang, R. G. Lorenzini, R. Ma, Q. Zhu, D. W. Sinkovits, G. Pilania, A. R. Oganov, S. Kumar, G. A. Sotzing, *et al.*, *Nat. Commun.*, 2014, **5**, 4845.
26 N. Drebov, A. Martinez-Limia, L. Kunz, A. Gola, T. Shigematsu, T. Eckl, P. Gumbsch and C. Elsässer, *New J. Phys.*, 2013, **15**, 125023.
27 M. R. Filip, G. E. Eperon, H. J. Snaith and F. Giustino, *Nat. Commun.*, 2014, **5**, 5757.
28 M. R. Filip and F. Giustino, *J. Phys. Chem. C*, 2016, **120**, 166–173.
29 C. H. Hendon, R. X. Yang, L. A. Burton and A. Walsh, *J. Mater. Chem. A*, 2015, **3**, 9067–9070.
30 T. J. Jacobsson, M. Pazoki, A. Hagfeldt and T. Edvinsson, *J. Phys. Chem. C*, 2015, **119**, 25673–25683.
31 F. El-Mellouhi, E. T. Bentria, S. N. Rashkeev, S. Kais and F. H. Alharbi, arXiv preprint arXiv:1604.06875, 2016.
32 F. El-Mellouhi, E. T. Bentria, A. Marzouk, S. N. Rashkeev, S. Kais and F. H. Alharbi, arXiv preprint arXiv:1604.07150, 2016.
33 L. Jiang, T. Wu, L. Sun, Y.-J. Li, A.-L. Li, R.-F. Lu, K. Zou and W.-Q. Deng, *J. Phys. Chem. C*, 2017, **121**, 24359–24364.
34 X. Meng, R. Zhang, Z. Fu and Q. Zhang, *Phys. Chem. Chem. Phys.*, 2016, **18**, 27358–27365.
35 H. Glawe, A. Sanna, E. K. U. Gross and M. A. L. Marques, *New J. Phys.*, 2016, **18**, 093011.
36 C. C. Stoumpos, C. D. Malliakas and M. G. Kanatzidis, *Inorg. Chem.*, 2013, **52**, 9019–9038.
37 https://en.wikipedia.org/wiki/List_of_oxidation_states_of_the_elements, 2018, https://en.wikipedia.org/wiki/List_of_oxidation_states_of_the_elements.
38 G. Kresse and J. Furthmüller, *Comput. Mater. Sci.*, 1996, **6**, 15–50.
39 J. P. Perdew, K. Burke and M. Ernzerhof, *Phys. Rev. Lett.*, 1996, **77**, 3865–3868.
40 I. E. Castelli, J. M. García-Lastra, K. S. Thygesen and K. W. Jacobsen, *APL Mater.*, 2014, **2**, 081514.
41 A. Jain, S. P. Ong, G. Hautier, W. Chen, W. D. Richards, S. Dacek, S. Cholia, D. Gunter, D. Skinner, G. Ceder and K. A. Persson, *APL Mater.*, 2013, **1**, 011002.
42 C. B. Barber, D. P. Dobkin and H. Huhdanpaa, *ACM Trans. Math Software*, 1996, **22**, 469–483.
43 J. E. Saal, S. Kirklin, M. Aykol, B. Meredig and C. Wolverton, *JOM*, 2013, **65**, 1501–1509.
44 J. Heyd, G. E. Scuseria and M. Ernzerhof, *J. Chem. Phys.*, 2003, **118**, 8207–8215.
45 G. K. Madsen and D. J. Singh, *Comput. Phys. Commun.*, 2006, **175**, 67–71.
46 K. Galkowski, A. Mitioglu, A. Miyata, P. Plochocka, O. Portugall, G. E. Eperon, J. T.-W. Wang, T. Stergiopoulos, S. D. Stranks, H. J. Snaith, *et al.*, *Energy Environ. Sci.*, 2016, **9**, 962–970.
47 K. Momma and F. Izumi, *J. Appl. Crystallogr.*, 2011, **44**, 1272–1276.